Proton radioactivity from proton-rich nuclei

F. Guzmán and M. Gonçalves*†

Instituto Superior de Ciências y Tecnologia Nucleares—ISCTN

Av. Salvador Allende y Luaces, Apartado Postal 6163, La Habana, Cuba.

O. A. P. Tavares and S. B. Duarte

Centro Brasileiro de Pesquisas Físicas—CBPF/CNPq

Rua Dr. Xavier Sigaud 150, 22290-180 Rio de Janeiro—RJ, Brazil.

F. García‡ and O. Rodríguez‡

Instituto de Física, Universidade de São Paulo

Caixa Postal 66318, 05315-970, São Paulo—SP, Brazil.

(March 12, 1999)

Half-lives for proton emission from proton-rich nuclei have been calculated by using the effective liquid drop model of heavy-particle decay of nuclei. It is shown that this model is able to offer results for spontaneous proton-emission half-life-values in excellent agreement with the existing experimental data. Predictions of half-life-values for other possible proton-emission cases are presented for null orbital angular momentum.

---

*Permanent address: Instituto de Radioproteção e Dosimetria, Av. Salvador Allende s/n, 22780-160 Rio de Janeiro—RJ, Brazil.

†Author to whom correspondence should be addressed: telo@ird.gov.br.

‡Permanent address: Instituto Superior de Ciências y Tecnologia Nucleares—ISCTN, Av. Salvador Allende y Luaces, Apartado Postal 6163, La Habana, Cuba.

In recent years new half-life measurements have been performed to better understand the proton and alpha decay processes in the region of proton-rich nuclei. These data are very promising for the analysis of possible irregularities in the structure of these proton-rich nuclei [1–11]. They are also of great interest in rapid proton capture nucleosynthesis processes. Some new results for proton radioactivity in this region of proton-rich nuclei have indicated that the proton emission mode is rather competitive with the alpha decay one [2,12,13].

The processes of alpha decay, cluster radioactivity, and cold fission have been already studied by us in the framework of the effective liquid drop model, and results have indicated that these three decay modes can be treated in a unified manner by this theoretical approach. In spite of using only gross nuclear properties, and one or two parameters (depending on which process is being described), the effective liquid drop model has given predicted half-life-values in pretty good agreement with the data for half-lives and yields for the three processes mentioned above [14–19].

In the present work we show that the effective liquid drop model has worked well when applied to the phenomenon of proton emission of nuclei in the proton-rich region. Half-life predictions for this process in the region of proton drip line can help in planning for further experiments to detect new proton-emitter nuclei. In what follows we briefly report the basic ingredients of the calculation.

In our model the Gamow penetrability factor,

$$\mathcal{P} = \exp\left\{-\frac{2}{\hbar}\int_{\zeta_0}^{\zeta_C}\sqrt{2\mu\,(V-Q)}d\zeta\right\} \quad , \tag{1}$$

is calculated under the current assumptions for shape parametrization and inertia coefficient of the fragments during the molecular phase of the decay [14–19]. The inner and outer turning points, ζ_0 and ζ_C respectively, are determined by using the experimental Q-value of the decay. The potential energy, $V(\zeta)$, is the sum of the Coulomb plus an effective surface term for the drop, where nuclear structure effects are included by means of the experimental Q-value, which value is an input data for the potential barrier calculation. The numerical

code which deals with alpha decay, cluster radioactivity, and cold fission processes is available from the library of the Queen's University of Belfast [20].

The effective liquid drop potential barrier in the case of proton decay of heavy nuclei, exhibits a small inner tail (Fig. 1). However, this tail remains a representative contribution from the inner part of the potential to the total penetrability factor calculation in the case of intermediate-mass proton emitters (from 5 up to 20% of the total Gamow's area). This contribution depends upon the inertia coefficient chosen to describe the decay process [14–17], as can be seen in Fig. 2. Here, Werner-Wheeler's and the effective inertia coefficients are shown as a function of the relative configuration of the system for the varying mass asymmetry shape (VMAS) and constant mass asymmetry shape (CMAS) parametrizations.

By using the current model, the half-lives for proton emission from proton-rich nuclei measured recently have been calculated and compared with experimental data as shown in Fig. 3. The present results are seen to agree agreement with the data, the largest difference between calculated and measured half-life-values, in the great majority of cases, being lower than one order of magnitude. The present half-life results have been obtained by using the VMAS shape parametrization combined with the effective inertia coefficient of Refs. [14–17]. Here, we have used the model parameter-values $r_0 = 1.38$ fm and $\lambda_0 = 5 \times 10^{20}$ s^{-1}, where r_0 is the nuclear radius parameter of the parent nucleus, $R = r_0 A^{1/3}$, and λ_0 is a parameter associated with the frequency of assaults on the potential barrier. Similar agreement between the model predictions and the data can be achieved for the other combinations of shape parametrization and inertia coefficient with a proper choice for model parameters r_0 and λ_0.

We remark that the contribution from the centrifugal barrier to the total potential barrier is relevant for light fragment emission processes [18,19], being even more significant for proton radioactivity. In fact, we have only attained good agreement with the data shown in Fig. 3 after including the experimental orbital angular momentum value, ℓ, into the calculation. Figure 4 shows the importance of the centrifugal barrier in calculating the half-life-values for proton emission from tantalum, rhenium and gold proton-rich isotopes in order to demonstrate the decisive role of the centrifugal barrier in the calculation. We

can clearly see that the orbital angular momentum in the decay is a key quantity to explore peculiarities in the shell structure of the proton-rich nuclei involved in the process. In addition, we note that the measured half-lives for proton decay of ^{156}Ta, ^{161}Re and ^{171}Au isotopes are reproduced by the current model only if angular momentum values different from those obtained from the experiment are used in the calculation. In fact, we have used $\ell = 2$, 3 and 4, instead of using the experimental values $\ell = 2$, 0, and 5, respectively, for ^{156}Ta, ^{161}Re, and ^{171}Au.

As mentioned earlier the purpose of this work is to give new theoretical, indicative half-life-values to further experimental prospecting of new proton emitters in the proton-drip line region. To this aim we have extended the present calculation to include all available mass-values of parent and daughter nuclei from the Atomic Mass Table by Audi *et al.* [21]. Results are presented in Table 1 together with available experimental data. Table 1 lists 24 cases of proton emitters in the half-life range of $\sim 1\mu$s–100 s. We remark that these theoretical estimates have been obtained with null orbital angular momentum ($\ell = 0$). They should be seen only as gross tentative to determine the experimental half-life-value of decay, since the proton emissions observed up to now have presented orbital angular momentum values differing significantly from null values. It should be mentioned that different alternative theoretical treatments to proton emission from nuclei in the spherical approximation have been recently investigated by Aberg *et al.* [22]

In conclusion, we have shown that the effective liquid drop model proved to be successful to predict the half-life for alpha decay, cluster radioactivity, and spontaneous cold fission processes of nuclei. The model also gives half-life-values which are in good agreement with the existing data for proton emission from proton-rich nuclei. Such calculated results can be treated as useful information to predict proton-decay half-lives of nuclei in this region. Results presented in Table 1 show that there are a number of proton decay cases which can be observed with attainable half-life values.

Acknowledgment

The authors would like to express their gratitude to the Brazilian CNPq, FAPESP,

FAPERJ, and CLAF for partial support.

---

[1] C. N. Davids *et al.*, Phys. Rev. Lett. **76**, 592 (1996).

[2] R. D. Page, P. J. Woods, R. A. Cunningham, T. Davinson, N. J. Davis, A. N. James, K. Livingston, P. J. Sellin, and A. C. Shotter, Phys. Rev. C **53**, 660 (1996).

[3] S. Hofmann, Radiochimica Acta **70/71**, 93 (1995).

[4] R. J. Tighe, D. M. Moltz, J. C. Batchelder, T. J. Ognibene, M. W. Rowe, and J. Cerny, Phys. Rev. C **49**, R2871 (1994).

[5] R. D. Page, P. J. Woods, R. A. Cunningham, T. Davinson, N. J. Davis, A. N. James, K. Livingston, P. J. Sellin, and A. C. Shotter, Phys. Rev. Lett. **72**, 1798 (1994).

[6] P. J. Woods, T. Davinson, N. J. Davis, S. Hofmann, A. N. James, K. Livingston, R. D. Page, P. J. Sellin, and A. C. Shotter, Nucl. Phys. **A553**, 485c (1993).

[7] K. Livingston, P. J. Woods, T. Davinson, N. J. Davis, S. Hofmann, A. N. James, R. D. Page, P. J. Sellin, and A. C. Shotter, Phys. Lett. **B312**, 46 (1993).

[8] K. S. Toth, D. C. Sousa, P. A. Wilmarth, J. M. Nitschke, and K. S. Vierinen, Phys. Rev. C **47**, 1804 (1993).

[9] A. Gillitzer, T. Faestermann, K. Hartel, P. Kienle, and E. Nolte, Z. Phys. **A326**, 107 (1987).

[10] T. Faestermann, A. Gillitzer, K. Hartel, P. Kienle, and E. Nolte, Phys. Lett. **B137**, 23 (1984)

[11] S. Hofmann, W. Reisdorf, G. Münzenberg, F. P. Hessberger, J. R. H. Schneider, and P. Armbruster, Z. Phys. A **305**, 111 (1982).

[12] T. Enqvist, K. Eskola, A. Jokinen, M. Leino, W. H. Trzaska, J. Uusitalo, V. Ninov, and P. Armbruster, Z. Phys. A **354**, 1 (1996).

[13] M. Leino *et al.*, Z. Phys. A **355**, 157 (1996).

[14] O. Rodríguez, F. Guzmán, S. B. Duarte, O. A. P. Tavares, F. García, and M. Gonçalves, Phys. Rev. C **59**, 253 (1999).

[15] O. A. P. Tavares, S. B. Duarte, O. Rodríguez, F. Guzmán, M. Gonçalves, and F. García, J. Phys. G: Nucl. Part. Phys. **24**, 1757 (1998).

[16] S. B. Duarte, O. Rodríguez, O. A. P. Tavares, M. Gonçalves, F. García, and F. Guzmán, Phys. Rev. C **57**, 2516 (1998).

[17] S. B. Duarte, M. G. Gonçalves, and O. A. P. Tavares, Phys. Rev. C **56**, 3414 (1997).

[18] S. B. Duarte and M. G. Gonçalves, Phys. Rev. C **53**, 2309 (1996).

[19] M. Gonçalves and S. B. Duarte, Phys. Rev. C **48**, 2409 (1993).

[20] M. Gonçalves, S. B. Duarte, F. García, and O. Rodríguez, Compt. Phys. Commun. **107**, 246 (1997).

[21] G. Audi, O. Bersillon, J. Blachot, and A. H. Wapstra, Nucl. Phys. A **624**, 1 (1997).

[22] S. Aberg, P. B. Semmens, and W. Nazarewicz, Phys. Rev. C **56**, 1762 (1997).

[23] P. J. Sellin, P. J. Woods, T. Davinson, N. J. Davis, K. Livingston, R. D. Page, A. C. Shotter, S. Hofmann, and A. N. James, , Phys. Rev. C **47**, 1933 (1993).

[24] O. Klepper, T. Batsch, S. Hofmann, R. Kirchner, W. Kurcewicz, W. Reisdorf, E. Roeckl, D. Schardt, and G. Nyman, Z. Phys. A **305**, 125 (1982).

[25] R. D. Page, P. J. Woods, R. A. Cunningham, T. Davinson, N. J. Davis, S. Hofmann, A. N. James, K. Livingston, P. J. Sellin, and A. C. Shotter, Phys. Rev. Lett. **68**, 1287 (1992).

[26] R. J. Irvine *et al.*, Phys. Rev. C **55**, R1621 (1997).

[27] C. N. Davids *et al.*, Phys. Rev. C **55**, 2255 (1997).

Figure captions:

Fig. 1: Effective potential barrier for proton radioactivity of ^{156}Ta isotope. The shaded area shows the inner tail of the potential constructed with the effective inertia coefficient and the VMAS for the shape parametrization (see Refs. [14–17]).

Fig. 2: Inertia coefficient for the process $^{156}\mathrm{Ta} \rightarrow \mathrm{p} + {}^{155}\mathrm{Hf}$. The figure shows the difference between various inertia coefficients for the molecular phase of the process. According to Refs. [14–17], model combinations are as follows: Werner-Wheeler inertia and VMAS description (solid line), Werner-Wheeler inertia and CMAS description (dashed line), effective inertia and VMAS description (dotted line), and effective inertia and CMAS description (dot-dashed line).

Fig. 3: Half-lives for proton radioactivity of proton-rich parent nuclei. The present calculated results (open squares) agree quite well with the experimental data (filled circles). Small deviations are seen only in a few cases where the difference between calculated and experimental values is larger than one order of magnitude. Data are those listed in Table 1.

Fig. 4: Angular momentum dependence of the half-life for proton radioactivity. Half-life calculations for ^{156}Ta (solid line), ^{161}Re (dashed line), and ^{171}Au (dotted line) isotopes change up to about ten orders of magnitude when orbital angular momentum varies from 0 to $10\hbar$. We display as filled symbols the experimental data for ^{156}Ta decay with $\ell = 2$ (circle), ^{161}Re decay with $\ell = 0$ (square), and ^{171}Au decay with $\ell = 5$ (diamond).

Table I: Half-life ($\log_{10}\tau$ [s]) for all measurable cases for proton emission from nuclei. The present half-life-values have been obtained by using the effective inertia coefficient in the VMAS shape parametrization, $\mu_{\text{eff.}}^{\text{VMAS}}$, with model parameter values $r_0 = 1.38$ fm, $\lambda_0 = 5 \times 10^{20}$ s^{-1}, and null orbital angular momentum. In the cases where the experimental half-life is available the reported ℓ-values are those to give the best agreement between calculated and measured half-life-values.

Parent		Half-life-values, $\log_{10}(\tau)$ [s]	
nucleus	ℓ	calculated	experimental
$^{55}_{29}$Cu	0	−5.22	—
$^{58}_{32}$Ge	0	−0.40	—
$^{105}_{51}$Sb	2	2.06	1.70 [4]
$^{109}_{53}$I	2	−4.46	−4.00 [9,10,23]
$^{112}_{55}$Cs	2	−3.58	−3.30 [5]
$^{113}_{55}$Cs	2	−5.91	−4.77 [5,9]
$^{142}_{67}$Ho	0	0.34	—
$^{146}_{69}$Tm	5	−0.69	−0.63 [7]
$^{147}_{69}$Tm	5	0.19	0.43 [8,23,24]
$^{150}_{71}$Lu	5	−1.74	−1.40 [6,23]
$^{151}_{71}$Lu	5	−1.44	0.89 [11,23]
$^{156}_{73}$Ta	2	−0.93	−0.84 [2,25]
$^{157}_{73}$Ta	0	−1.22	−0.52 [26]
$^{160}_{75}$Re	2	−3.48	−3.06 [25]
$^{161}_{75}$Re	3	−3.64	−3.43 [26]
$^{165}_{77}$Ir	5	−4.17	−3.46 [27]
$^{166}_{77}$Ir	2	−0.98	−0.82 [27]
$^{167}_{77}$Ir	0	−1.55	−0.96 [27]
$^{171}_{79}$Au	4	−3.22	−2.65 [27]
$^{177}_{81}$Tl	0	−5.00	—
$^{178}_{81}$Tl	0	1.57	—
$^{179}_{81}$Tl	0	0.06	—
$^{185}_{83}$Bi	0	−4.89	−4.35 [1]
$^{187}_{83}$Bi	0	−1.53	—

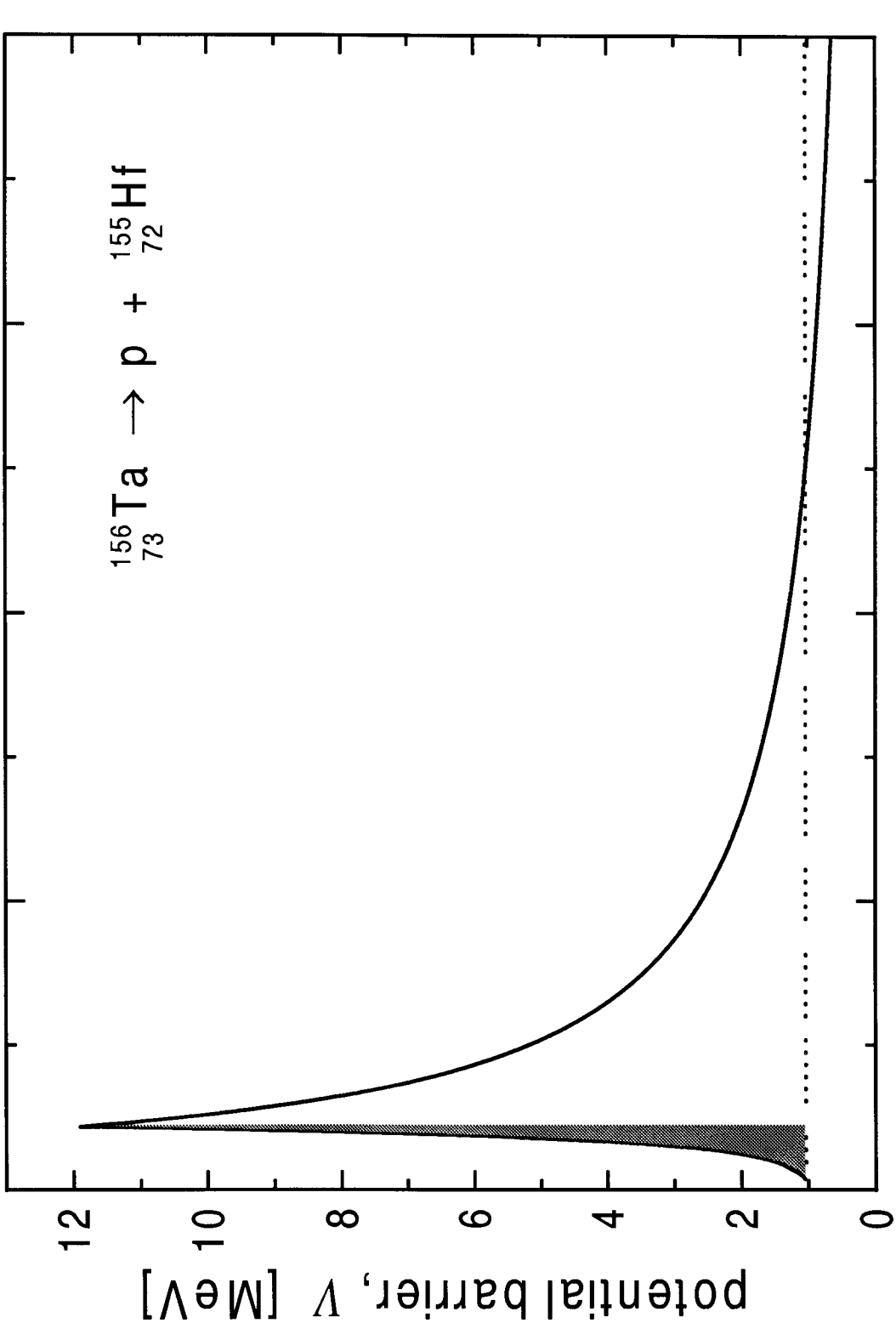

Fig. 1
Guzman *et al.*

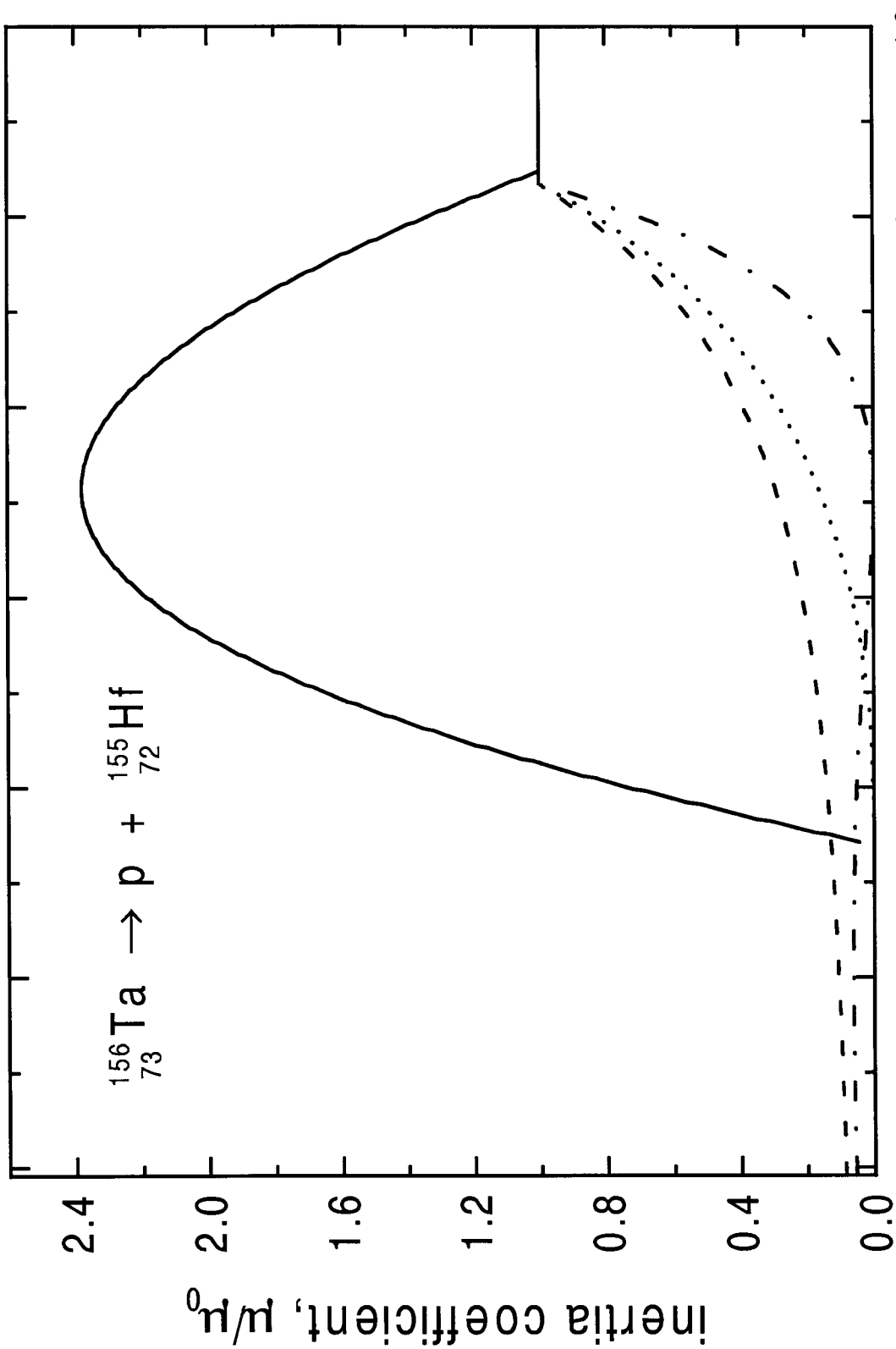

Fig. 2
Guzman *et al.*

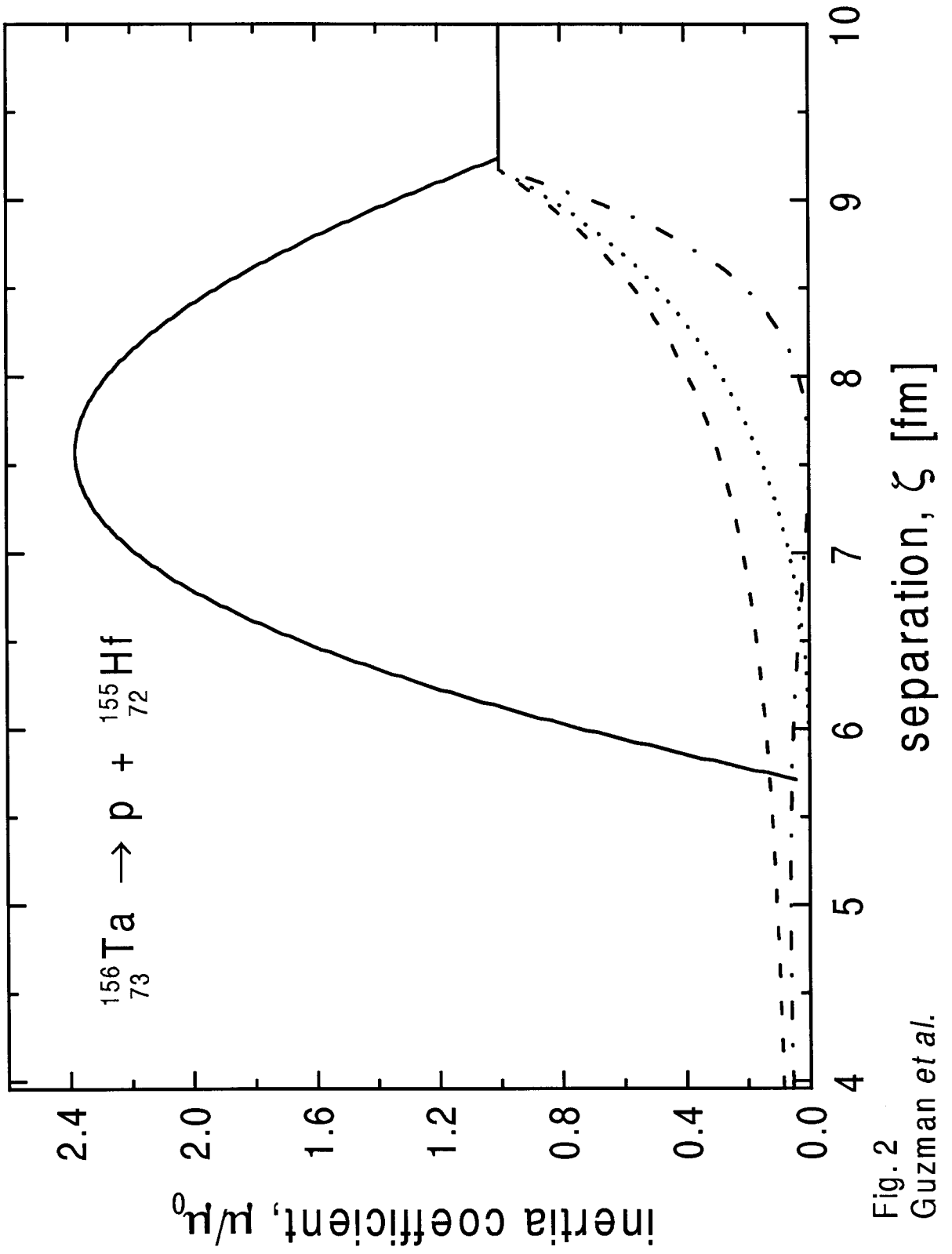

Fig. 2
Guzman *et al.*

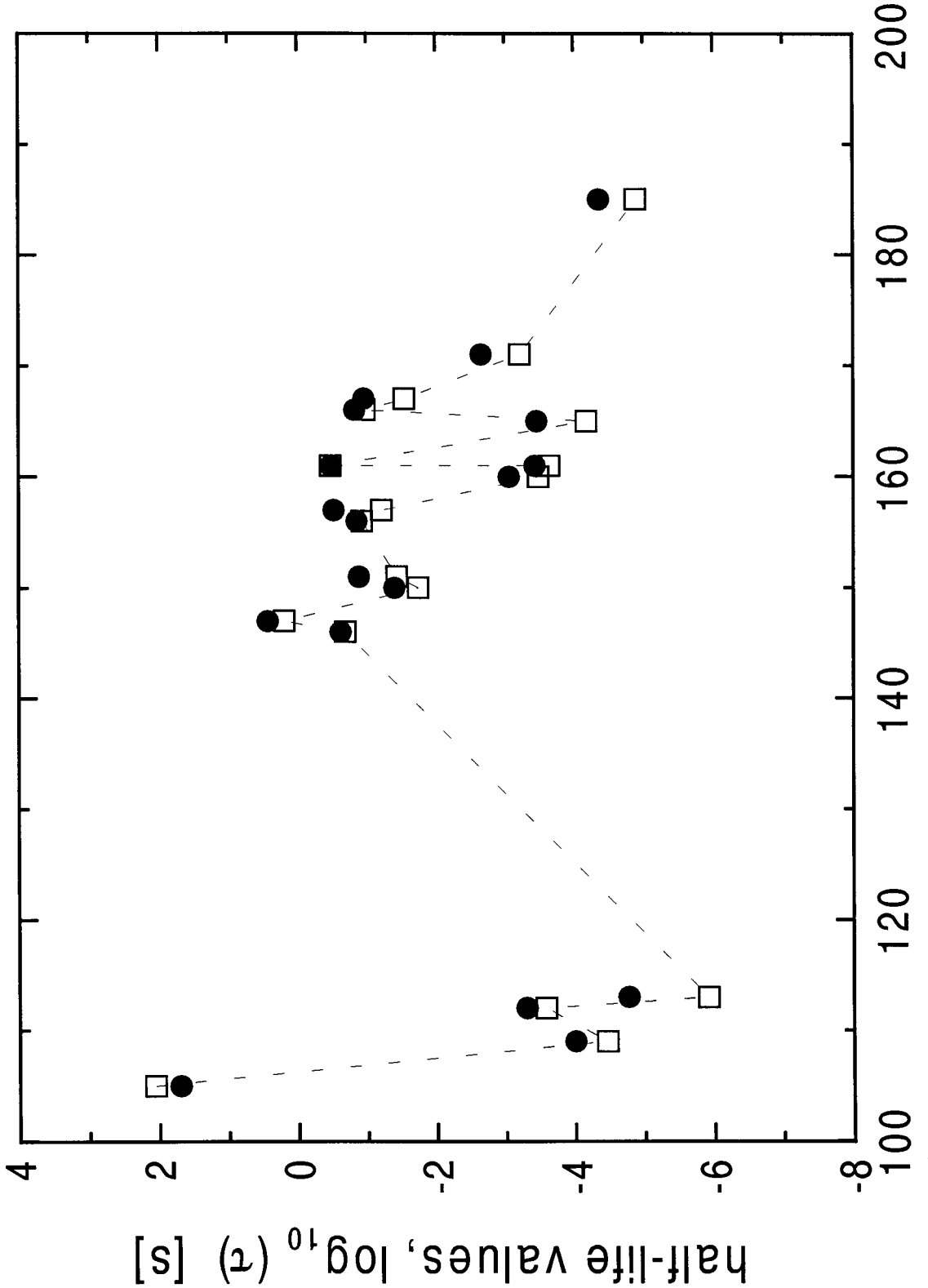

Fig. 3
Guzman *et al.*

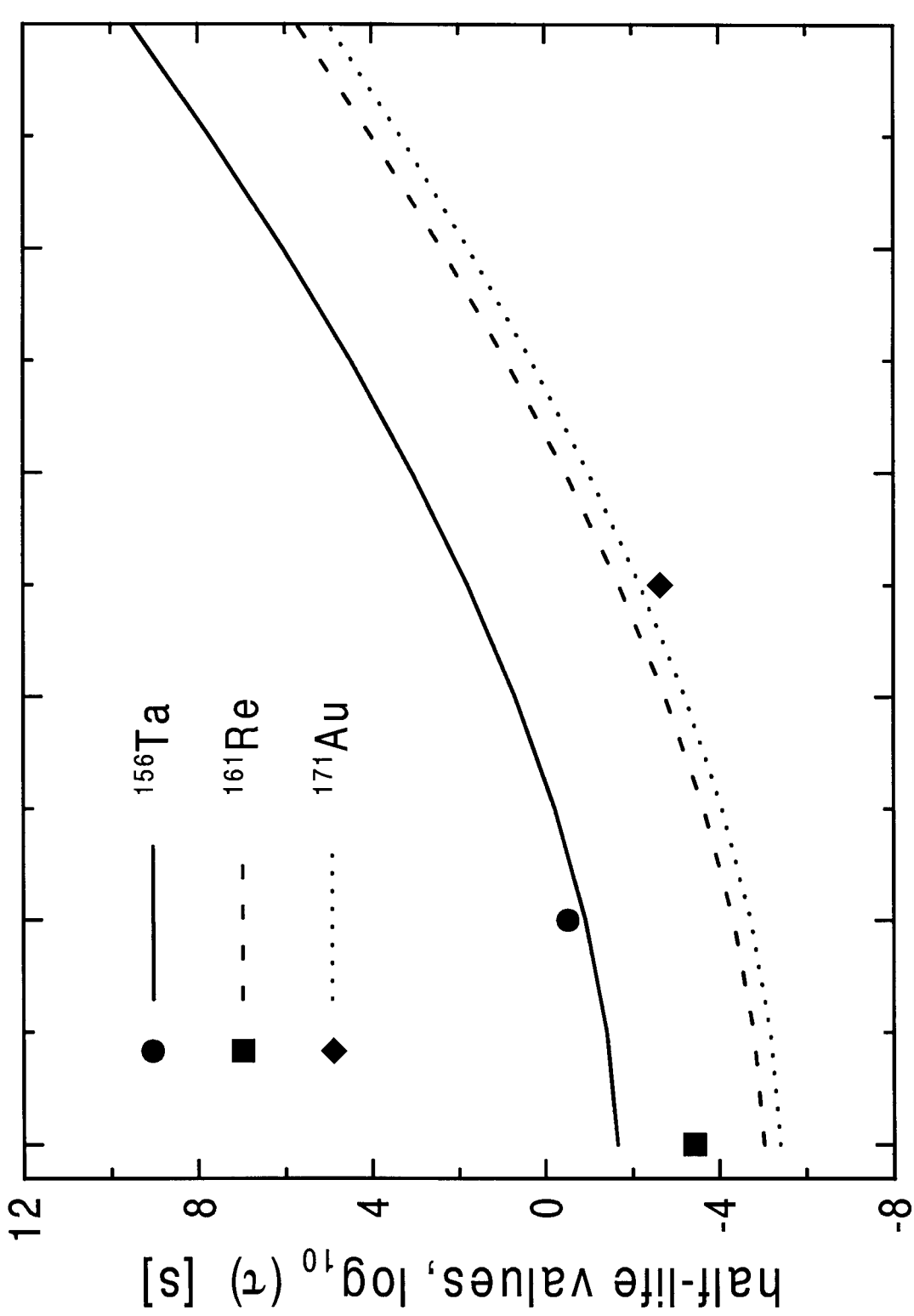

Fig. 4
Guzman *et al.*